Inhomogeneous magnetization transfer imaging: Concepts and directions for further development

David Alsop, Ece Ercan, Olivier Girard, Alex Mackay, Carl Michal, Gopal Varma, Elena Vinogradov, Guillaume Duhamel

Inhomogeneous Magnetization Transfer (ihMT) Imaging: Concepts and Directions for Further Development

David C. Alsop[1], Ece Ercan[2], Olivier M. Girard[3], Alex L. Mackay[4,5], Carl A. Michal[4], Gopal Varma[1], Elena Vinogradov[6], Guillaume Duhamel[3]

[1]Department of Radiology, Beth Israel Deaconess Medical Center and Harvard Medical School, Boston, MA USA.
[2]MR Clinical Science, Philips, Best, The Netherlands.
[3]Aix Marseille Univ, CNRS, CRMBM, Marseille, France.
[4]Department of Physics and Astronomy, University of British Columbia, Vancouver, BC, Canada.
[5]Department of Radiology, University of British Columbia, Vancouver, BC, Canada.
[6]Department of Radiology and Advanced Imaging Research Center, UT Southwestern Medical Center, Dallas, TX, USA.

Abstract:

Off resonance RF irradiation can induce the ordering of proton spins in the dipolar fields of their neighbors, in molecules with restricted mobility. This dipolar order decays with a characteristic relaxation time, T_{1D}, that is very different from the T1 and T2 relaxation of the nuclear alignment with the main magnetic field. Inhomogeneous Magnetization Transfer (ihMT) imaging is a refinement of Magnetization Transfer (MT) imaging that isolates the MT signal dependence on dipolar order relaxation times within motion constrained molecules. Since T_{1D} relaxation is a unique contrast mechanism, ihMT may enable improved characterization of tissue. Initial work has stressed the high correlation between ihMT signal and myelin density. Dipolar order relaxation appears to be much longer in membrane lipids than other molecules. Recent work has shown, however, that ihMT acquisitions may also be adjusted to emphasize different ranges of T_{1D}. These newer approaches may be sensitive to other

microstructural components of tissue. Here we review the concepts and history of ihMT and lay out needs for further development to realize its full potential.

Inhomogeneous magnetization transfer imaging(1), or ihMT, is a refinement of magnetization transfer that provides different contrast between tissues than MT by isolating dipolar order effects within motion restricted molecules(2) that are weighted by the corresponding dipolar relaxation time, T_{1D}. Because dipolar order relaxation is slower in myelinated tissues than any other tissue observed, it is highly sensitive to myelin. More broadly, the addition of a new relaxation mechanism for MRI that reflects macromolecular structure and mobility and with clearly different properties from T_1 and T_2 opens the possibility of heightened sensitivity to pathology.

Though a growing body of literature describes the properties of ihMT MRI, much work remains to realize its potential for research and clinical studies. After a brief introduction, this review is organized around 6 major directions for further investigation and development: 1. Determining the underlying physics and tissue parameters behind ihMT; 2. Estimating, validating, separating, and interpreting different T_{1D} components; 3. Optimizing acquisition methods; 4. Optimizing quantification methods; 5. Validating ihMT measures; 6. Disseminating standard methods and evaluating them in different pathologies.

Introduction to ihMT

Decades of work have shown the important contribution of magnetization exchange between mobile water and motionally constrained molecules (MCMs) to relaxation times in tissue(3). The magnetization exchange is exploited in magnetization transfer (MT) imaging, where off-resonance RF irradiation is used to preferentially saturate the “immobile” protons(4). Rapid magnetization exchange with water is facilitated by spin diffusion along the molecules to rapidly exchanging amine and hydroxyl protons(5). MCMs generally have very short T_2s, on the order of tens of microseconds, because of the strong dipolar interaction between nearby protons. Unlike mobile protons in water, where rapid diffusion and isotropic rotation greatly attenuate proton-proton coupling effects on T_2 and the lineshape, immobile MCM protons retain a residual dipolar coupling. MCM lineshapes are very broad and not Lorentzian in shape(6,7). Indeed, the NMR properties of the MCM protons are more typical of solid state NMR than solution NMR(8).

These solid-like NMR lines have another important difference from solution NMR; the extended proton dipolar coupling network allows for a sustained nonzero dipolar interaction energy. This energy is described by a part of the spin Hamiltonian that is separable from (i.e. commutes with) the Zeeman interaction between spins and the main magnetic field. Nonzero dipolar energy reflects the extent of ordering of proton spins within the fields of their local dipolar couplings(9). A simple and rather

intuitive illustration of such order can be seen in an ensemble of two coupled proton spins as illustrated in figure 1. The energy levels of two strongly coupled identical spin ½ protons consist of a spin-1 triplet having energy levels with different z angular momentum projections, m=1, 0,-1 (shown as $|T_{0,+1,-1}\rangle$ in figure 1) and a spin-0 singlet level ($|S_0\rangle$) that does not couple to the main magnetic field. Depending on the angle between the vector connecting the spins and the magnetic field, the spin interaction either raises or lowers the energy of the m=+1 and m=-1 triplet levels, while the m=0 level is shifted oppositely. This splits the line into two symmetrically shifted lines, known as a Pake doublet(10). Irradiation at the center of one of the lines saturates that line but also increases the population difference between the levels of the other line, resulting in a 50% enhancement of this other line(11) when observed with small flip angle excitation pulses. (Perhaps surprisingly, the asymmetry is not observable if a broadband 90° pulse is used to excite the NMR signals because it will excite a symmetric doublet(12)). The asymmetry of the line after saturation reflects dipolar order. Such dipolar order is also known to relax to equilibrium with a distinct dipolar relaxation time, T_{1D}, that is typically intermediate between T_2 and T_1. The equilibrium dipolar order is usually approximated as zero because thermal and Zeeman energies are so much larger than the dipolar interaction energy. The key concept underlying the existence of dipolar order within coupled spin systems is the existence of additional degrees of freedom within the energy level distribution, as compared to the conventional liquids NMR model of an ensemble of isolated spin-½ nuclei for which dipolar order does not exist. The Zeeman energy depends on the total numbers of up and down spins, while the dipolar energy depends upon how those up and down spins are distributed in space in each other's local fields.

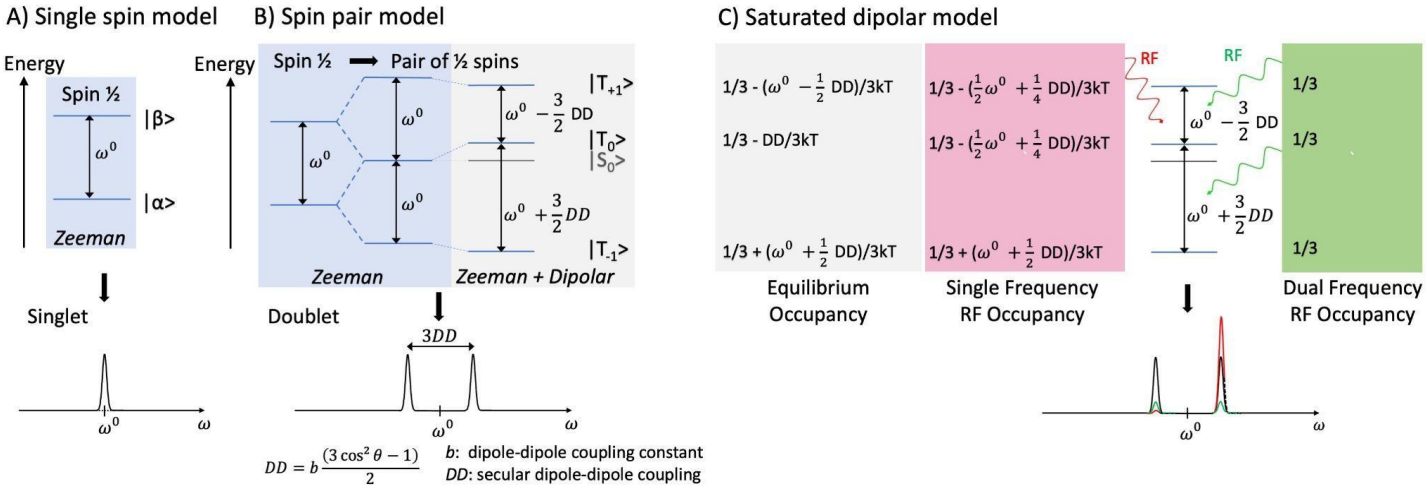

Figure 1: Dipolar order effects in a two spin system. A) a single spin half nucleus produces a single line. B) When two spins interact strongly, their energy levels separate into 3 triplet energy states ($|T_{0,+1,-1}\rangle$) and one NMR insensitive singlet, ($|S_0\rangle$). The

dipolar interaction shifts the energy of the levels slightly, leading to two transitions with frequencies equally spaced from the single spin frequency. C) Single frequency RF irradiation at the frequency of the transition between the two higher energy levels saturates that line, but also increases the intensity of the other line by 50% by reducing the occupancy of the triplet zero state. Overall single frequency saturation of magnetization is just 25% effective. Simultaneous dual frequency RF saturation of both lines fully saturates magnetization.

The search for a potential contribution of dipolar order and dipolar order relaxation to MT studies has a long history. Theoretical models for inclusion of dipolar order in MT studies were proposed by Yang and Schleich(13) and Yeung, Adler and Swanson(14). A dipolar reservoir was included in a super-Lorentzian lineshape model by Morrison and Henkelman(15) and used to fit data obtained from membrane suspensions and ex-vivo bovine white matter at room temperature. The effect of dipolar order in these fits was small, and tissue T_{1D}s were less than 1ms. Studies performed on protein and agar gels(16,17) similarly found a very small effect and concluded that dipolar order effects may be neglected in MT imaging experiments. But in 2004, Alsop et al. (18) reported an unexpected artifact in a particular Arterial Spin Labeling subtraction strategy that was greatest in white matter. Much further study and evaluation led to eventual publication by Varma et al.(1) of the inhomogeneous magnetization transfer effect. Two key differences from the previous MT studies contributed to the more positive finding. The first was the use of a subtraction experiment between images acquired with single frequency irradiation and those acquired with power evenly split between positive and negative frequency offsets. As emphasized by Lee et al. (19), dual frequency irradiation effectively removes dipolar order effects and increases saturation of a dipolar coupled system. Comparison with single frequency irradiation(1), which includes these effects, isolates dipolar order contributions (Figure 2). The second difference was acquisition of brain data in-vivo at body temperature; later studies have shown that white matter T_{1D} is highly temperature sensitive(20,21). Under in-vivo conditions in humans, the dual frequency MT ratio in white matter is approximately 3 to 5% greater than that for single frequency MT(1,22,23). The detectability of ihMT effects in-vivo have recently been further increased with the introduction of sparse energy RF irradiation(24,25), that can increase the MT ratio difference in white matter by 2 to 3 fold.

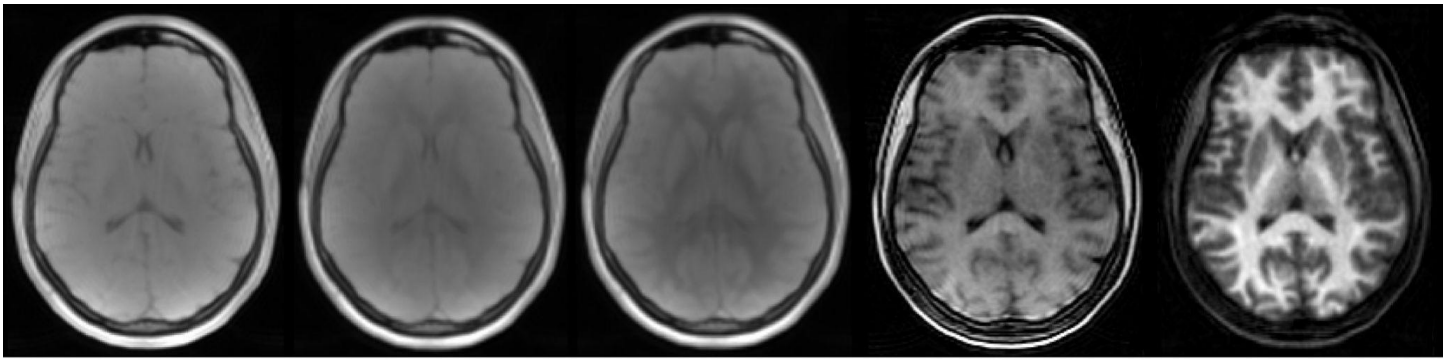

Figure 2. ihMT contrast is generated by subtraction of the signals (S) from single, S_+ and S_-, and dual frequency, $S_\pm$, saturated images. Conventional MT contrast subtracts a single frequency saturation image from a zero power reference. Greater contrast between gray and white matter in the ihMT image reflects a higher density of long T_{1D} spins in white matter.

Two definitions in the original publication of ihMT have been a subject of debate. The first is the name “inhomogeneous magnetization transfer”. This name was chosen(1) because it was thought that the magnetization on one side of the line was not tightly coupled to the other side, as occurs with broadening of a line by an inhomogeneous magnetic field. In other words, the line may not be considered a single entity as the transfer of energy within the line is not infinitely fast. However, the term “inhomogeneous broadening” has several other historical definitions. Portis(26) defined inhomogeneous broadening as any process where a system of identical spins was perturbed by local variations of an outside interaction. The definition was also motivated by analogy to an inhomogeneous magnetic field but was studied in the context of heterogeneous spin systems of Electron Spin Resonance. Later Maricq and Waugh(27) defined inhomogeneous broadening in the context of magic angle spinning NMR based on the rotational invariance (commutation property) of the Hamiltonian. According to these definitions, ihMT results from a homogeneous interaction, and it has been argued the name is inappropriate(12). However, both because the name has already been widely used in the literature, and because there is no brief, clearly recognized term for the long T_{1D} saturation effects it observes, the name ihMT has been retained here. A second debated definition in the original publication(1) was the ihMT ratio, defined as

$$ihMTR = \frac{S_+ + S_- - 2S_\pm}{S_0}, \quad [1]$$

where the S's reflect the image signal intensities, for positive frequency offset, +, negative frequency offset, -, and dual frequency offset with equal power, ±, irradiation. This measure was chosen because acquiring both positive and negative irradiation was desirable for removal of MT asymmetry and magnetic field nonuniformity effects(28). This definition effectively doubles the signal difference between single and dual frequency experiments and some have adopted the above value divided by two(21), but the original definition is retained here for consistency with past literature.

Unlike the simple two spin model, real world larger molecules of relevance to MRI contain many protons interacting with each other. Inter and intramolecular interactions strongly broaden the lines and many potential combinations of energy levels exist. Modeling individual energy levels is not possible. Fortunately, a simplifying thermodynamic theory(29) has proved successful in many solid state applications involving a large number of coupled spins and, so far, in ihMT studies. This approximation separates the energy, or Hamiltonian, of the system into the Zeeman interaction energy with the main magnetic field and the internal dipolar interaction energy. Under the high field and high temperature approximation, the energy reservoirs are then characterized by separate spin temperatures, independent of the sample temperature, with any deviation from a thermal distribution decaying on the timescale of T_2.

As first derived by Provotorov, the Zeeman and dipolar energy compartments, representing different interactions of the same motion restricted spins, are coupled upon application of single frequency RF. The dynamic equations, including the motion restricted pool (B) and an exchanging mobile water pool(A) are (adapting the notation of (15)):

$$\begin{pmatrix} \dfrac{d\beta}{dt} = R_{rf}^{B}\left(\dfrac{\omega}{D}\right)M_z^B - \left(\dfrac{1}{T_{1D}} + R_{rf}^{B}\left(\dfrac{\omega}{D}\right)^2\right)\beta \\ \dfrac{dM_z^B}{dt} = R_1^B\left(M_0^B - M_z^B\right) - R_{rf}^{B}\left(M_z^B - \left(\dfrac{\omega}{D}\right)\beta\right) - \left[R\left(M_z^B M_0^A - M_0^B M_z^A\right)\right] \end{pmatrix}_{motion\ restricted}$$

$$\left(\frac{dM_z^A}{dt} = R_1^A\left(M_0^A - M_z^A\right) - R_{rf}^{A}M_z^A - \left[R\left(M_0^B M_z^A - M_z^B M_0^A\right)\right]\right)_{mobile} \quad . \qquad [2]$$

Where β is proportional to the inverse spin temperature of dipolar order energy, $M_z^{A,B}$ are the z magnetizations of the mobile and motion restricted pools (conceptually proportional to the inverse spin temperature of the Zeeman order) and $M_0^{A,B}$ are their equilibrium values. T_{1D} is defined as the

decay time of dipolar order and D is the local dipolar field (in angular frequency units), corresponding to the averaged dipolar interaction within the coupled spin system that can be calculated as the square root of one third of the second moment of the lineshape(9). $R_1^{A,B}$ are the longitudinal relaxation rates of the two pools, and, ω is the angular frequency of the RF irradiation. The motion restricted pool exchange with the mobile pool is described by the exchange rate R. $R_{rf}^{A,B}$ are applied RF absorption rates defined by $R_{rf}^{A,B}=\pi\omega_1^2 g_{A,B}(\omega)$ where ω_1 is the RF amplitude in angular frequency units and $g_{A,B}(\omega)$ are the equilibrium absorption lineshapes of the mobile and motion restricted pools.

The presence of nonzero dipolar interaction energy effectively distorts the effective instantaneous absorption spectrum, or lineshape, of the motion restricted Zeeman line. As seen in line 2 of eq. [2], the effective instantaneous absorption spectrum becomes asymmetric in frequency

$$\tilde{R}_{rf}^{B}=\pi\omega_1^2\tilde{g}_B(\omega)=\pi\omega_1^2 g_B(\omega)\left(1-\left(\frac{\omega}{D}\right)\frac{\beta}{M_z^B}\right)=R_{rf}^{B}\left(1-\left(\frac{\omega}{D}\right)\frac{\beta}{M_z^B}\right), \qquad [3]$$

Where $\tilde{R}_{rf}^{B}$ and $\tilde{g}_B(\omega)$ are the effective absorption rate and lineshape modified by dipolar order. Note that if power is applied equally at positive and negative frequency so that their absorption contributions add, the dipolar order effects cancel to the extent that the equilibrium line is symmetric, usually a good first approximation. The saturation rate during dual-frequency irradiation is then given by

$$\begin{aligned}\tilde{R}_{rf\,dual}^{B}&=\frac{\pi\omega_1^2}{2}\left(\tilde{g}_B(\omega)+\tilde{g}_B(-\omega)\right)\\&=\frac{\pi\omega_1^2}{2}\left(g_B(\omega)+g_B(-\omega)-\left(\frac{\omega}{D}\right)\frac{\beta}{M_z^B}g_B(\omega)-\left(\frac{-\omega}{D}\right)\frac{\beta}{M_z^B}g_B(-\omega)\right)\\&=\frac{\pi\omega_1^2}{2}\left(g_B(\omega)+g_B(-\omega)-\left(\frac{\omega}{D}\right)\frac{\beta}{M_z^B}\left(g_B(\omega)-g_B(-\omega)\right)\right)\\&\approx\pi\omega_1^2 g_B(\omega)\end{aligned} \qquad . \quad [4]$$

This means that the term involving dipolar order in line 2 of eq. [2] should be set to zero and dipolar order has no effect on magnetization when dual frequency irradiation is applied.

Insights can be gained by looking at the steady state solutions of eq. [2] for which the derivatives on the left are all zero. First, note that the steady state solution for the dipolar order is

$$\beta^{ss} = \frac{T_{1D} R_{rf}^{B} \left(\frac{\omega}{D} \right)}{\left(1 + T_{1D} R_{rf}^{B} \left(\frac{\omega}{D} \right)^{2} \right)} M_{z}^{B} \quad . \quad [5]$$

Substituting this in eq. [3] gives the steady state RF effective saturation rate

$$\tilde{R}_{rf\,single}^{Bss} = \frac{R_{rf}^{B}}{\left(1 + T_{1D} R_{rf}^{B} \left(\frac{\omega}{D} \right)^{2} \right)} \quad . \quad [6]$$

In the steady state, dipolar order effects simply reduce the effective RF saturation. In contrast, the saturation rate for dual frequency RF is unaffected by dipolar order as seen in eq. [4]

$$\tilde{R}_{rf\,dual}^{Bss} = R_{rf}^{B} \qquad [7]$$

The steady state magnetization of the free pool then depends on dipolar order and RF saturation of the motion restricted pool only through the corresponding effective saturation rate, $\tilde{R}_{rf}^{Bss}$, for single or dual frequency:

$$\frac{M_{z}^{Ass}}{M_{0}^{A}} = \left(1 + \frac{\left(R_{rf}^{A} + \tilde{R}_{rf}^{Bss} \left(\frac{RM_{0}^{B}}{R_{1}^{B} + RM_{0}^{A} + \tilde{R}_{rf}^{Bss}} \right) \right)}{\left(R_{1}^{A} + R_{1}^{B} \frac{RM_{0}^{B}}{R_{1}^{B} + RM_{0}^{A} + \tilde{R}_{rf}^{Bss}} \right)} \right)^{-1} \approx \left(1 + \frac{\left(R_{rf}^{A} + \tilde{R}_{rf}^{Bss} \left(\frac{RM_{0}^{B}}{R_{1}^{B} + RM_{0}^{A}} \right) \right)}{\left(R_{1}^{A} + R_{1}^{B} \frac{RM_{0}^{B}}{R_{1}^{B} + RM_{0}^{A}} \right)} \right)^{-1} \qquad [8]$$

This solution is analogous to the classical steady state solution of the binary spin bath model(15). The approximate solution on the right assumes exchange and possibly motion restricted pool relaxation are much faster than RF saturation, $\left(RM_{0}^{A} + R_{1}^{B} \right) >> R_{rf}^{A}, \tilde{R}_{rf}^{Bss}$, generally a good approximation for power constrained in-vivo human experiments at moderate to large frequency offsets. Note that dipolar order effects enter only through the dependence on $\tilde{R}_{rf}^{Bss}$. The effect of ihMT is simplest in this model if one subtracts the inverse of the magnetizations between the dual and single frequency acquisitions(25), giving

$$ihMTR_{inv} = \frac{2M_0^A}{M_{zdual}^{Ass}} - \frac{2M_0^A}{M_{zsingle}^{Ass}}$$

$$\approx 2\left(\frac{\left(\frac{RM_0^B}{R_1^B + RM_0^A}\right)}{R_1^A + R_1^B\left(\frac{RM_0^B}{R_1^B + RM_0^A}\right)}\right)\left(\tilde{R}_{rf\,dual}^{Bss} - \tilde{R}_{rf\,single}^{Bss}\right)$$

$$= 2\left(\frac{\left(\frac{RM_0^B}{R_1^B + RM_0^A}\right)}{R_1^A + R_1^B\left(\frac{RM_0^B}{R_1^B + RM_0^A}\right)}\right)\left(\frac{T_{1D}\left(R_{rf}^B\right)^2\left(\frac{\omega}{D}\right)^2}{1 + T_{1D}R_{rf}^B\left(\frac{\omega}{D}\right)^2}\right) \quad . \quad [9]$$

This $ihMTR_{inv}$ quantity is closely related to the more conventional ihMTR,

$$ihMTR = \frac{M_{zdual}^{Ass} M_{zsingle}^{Ass}}{\left(M_0^A\right)^2} ihMTR_{inv} \quad . [10]$$

As the term $T_{1D}R_{rf}^B\left(\frac{\omega}{D}\right)^2$ in eq. [9] approaches 1, the saturation of the motion restricted pool is reduced relative to dual frequency irradiation (eqs. [6] and [7]) and $ihMTR_{inv}$ increases. Hence this term is a measure of the contribution of dipolar order effects to single frequency saturation studies. For in-vivo applications, where power is often constrained by safety limits, the time average of this term is typically smaller than one (for example the term is 0.132 for a superlorentzian line with T_2 of 10μs and T_{1D} of 6ms typical of white matter and rms RF amplitude of 3μT applied 7kHz off resonance), though it may transiently exceed 1 if low duty cycle saturation is used. The difference in saturation of the motion restricted pool, after exchange with the free water pool, drives the ihMT effect (Figure 3).

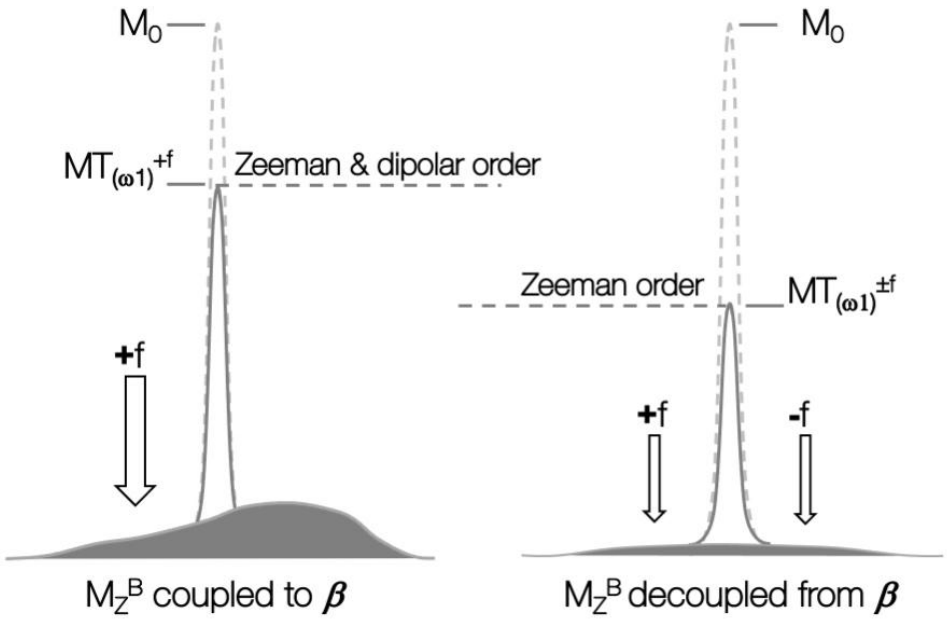

Figure 3: Differential effects of single and dual frequency saturation on the bound (gray) and mobile (white) pools. Single frequency (+f=ω/2π) RF couples the Zeeman magnetization to the dipolar order, making the bound pool line asymmetric and reducing the saturation efficiency of Zeeman magnetization in the bound and mobile pools. Dual frequency (±f) RF decouples Zeeman magnetization and dipolar order and achieves efficient saturation of bound and mobile pools.

Several important observations can be made from eq[9]. First is that the difference in magnetization is proportional to T_{1D}, so long T_{1D} systems will have the highest ihMT signal. The second is that ihMT increases relative to MT for large frequency offsets, comparable to or greater than the local field frequency, D, which also determines the width of the lineshape, g(ω). Third, the ihMT effect increases as the square of the RF power (i.e., ω_1^4) for modest powers. It has been shown that the ihMT effect can be increased relative to the steady state by applying short pulses of higher RF power but with low duty cycle so as to maintain the same time averaged power(24,25). This maximizes the time average of power squared for fixed power. Increases of 3 fold or more make this sparse power strategy an important approach for sensitive acquisitions in-vivo. The ω_1^4 dependence also indicates that any spatial nonuniformity of the RF field will introduce spatial variation in ihMT sensitivity. Finally, ihMT measured with different power, duty cycle, or offset frequencies will differ greatly, so care must be taken in comparing results reported with different values for these experimental parameters.

1. Determining the underlying physics and tissue parameters behind ihMT.

An important goal for studies of ihMT in tissue is to provide estimates of the key physical parameters responsible for ihMT. As we shall discuss in the subsequent paragraphs, the imperfect fitting of ihMT data to simpler models has complicated tissue parameter measurement and the current literature has not yet agreed on the values.

In principle, ihMT adds only one additional parameter to the two pool model frequently used for quantitative studies of MT(e.g. (15)), namely the dipolar order relaxation time T_{1D}. Varma et al.(2) reported the first fits of a two pool model with dipolar order to in-vivo ihMT data. The two pool model couples the bound pool system of eq [2] to a free water compartment by exchange. In a simultaneous fit to dual frequency magnetization transfer data and the difference between dual and single frequency, a plausible fit was obtained. Measured (human) T_{1D}s using this model were between 2.9 and 3.5 ms for white matter and ~1 ms for gray matter. Though the fits were sufficient to support the interpretation of ihMT as an effect of dipolar order, this model underfit the acquired data. The quality of the fits could be improved by adding an additional parameter to the model. The bound pool was divided into two parts: a fraction of the bound pool with nonzero T_{1D}. and the remainder having T_{1D} infinitesimally close to zero. The idea being that many molecular contributors to MT may have very short T_{1D} and only the fraction, f, perhaps representing the myelin contribution, has a longer T_{1D}. This additional parameter substantially improved the fits and greatly increased the measured T_{1D}s to roughly 40 ms in white matter and up to 48 ms in gray matter (with f values almost half of those in white matter), but with substantial uncertainty (with standard deviations as high as 16 ms). Hence this first report only loosely constrained brain T_{1D} measures to between 3 and 40 ms. Still, this range of times is shorter than the time required for complete exchange across cellular and other boundaries in tissue, raising the possibility that multiple pools may need to be modeled separately for better accuracy. Further studies constraining the distribution of T_{1D}s in tissue are reviewed in the next section.

In addition to the important role of T_{1D}, the bound pool lineshape becomes an important determinant of the ihMT signal as a function of power and frequency. Equation [9] shows that the ihMT signal difference depends on the square of the line shape. This is a stronger nonlinear dependence than for conventional MT. Deviations from assumed models, such as the super-Lorentzian lineshape, could substantially change model results. The super-Lorentzian lineshape is derived by averaging across a uniform angular distribution of molecular directions, but if the magnetization at different angles does not exchange rapidly relative to T_{1D} and the ihMT signal is nonlinear in the line shape, then averaging

of the line shapes may be inaccurate. An alternative model where different angles were considered as different pools that exchange with the free water was also considered in (2). This model, referred to as the Complete Angular Averaging model, provided better fits to the data in brain tissue, though it did not lead to qualitatively different results.

One important manifestation of the strong lineshape dependence of ihMT is an observed angular dependence of ihMT(1,23,30,31). Intramolecular dipolar couplings have a strong dependence on orientation. In a lipid bilayer where fast rotation of lipid molecules about the bilayer normal partially averages the dipolar couplings, they vanish at the magic angle of approximately 55° from the magnetic field direction. In oriented tissues like white matter, the assumption of uniform distribution in angle is not valid. The cylindrical distribution of molecules within an axon or myelin membrane, for example, will lead to a modification of the lineshape. Angular dependence of conventional MT has been reported and modeled(32), and a similar lineshape may be used to model ihMT data as well(31). The effect in ihMT is potentially stronger and will require more detailed study to separate angular effects from other tissue parameters. Measurements of the orientation dependence of ihMTR and T_{1D} in aligned lipid bilayers supported on glass slides show profound effects(33). For the parameters used there, ihMTR was found to have a roughly $\left(3\cos^2\theta - 1\right)^2$ dependence on the angle, θ, from the magnetic field.

2. Estimating, validating, separating, and interpreting different T_{1D} components

As described above, the ihMT technique is intrinsically weighted by T_{1D}, the dipolar relaxation time. T_{1D}-relaxation is driven by molecular motions and can deliver quantitative information about molecular dynamics and organization(34) with a specific sensitivity to slow motional processes such as lipid membrane collective motions(35) whose timescales (10^{-6} – 1 s) are not accessible with standard T_1 and T_2 relaxometry MRI.

In solid-state NMR, T_{1D} is often measured with a Jeener-Broekaert pulse sequence(36), which requires short, high amplitude pulses not accessible for in-vivo MRI. Jeener-Broekaert sequences measure the dipolar order effects directly in the bound pool, unlike ihMT where the effects are observed indirectly by exchange to the free pool. Jeener-Broekaert measurements in specimens can provide invaluable information on T_{1D} within tissue. Swanson et al.(20) reported Jeener-Broekaert measurements of T_{1D} (at 2.0 T) in formalin fixed bovine spinal cord white matter of 11.1 ms at 40°C and 1.9 ms at 20°C. While the data fitting for this measurement emphasized the longest decay times, the presence of substantial signal with shorter decay times suggests a T_{1D} distribution that includes

much shorter T_{1D}s. Though the effect of formalin fixation on ihMT is uncertain, these values provide important information on in-vivo T_{1D} in brain tissue.

Since modeling of power and frequency dependence of ihMT only loosely constrained T_{1D}, a refinement of the ihMT sequence to improve in-vivo T_{1D} measurement was needed. Subsequently, it was found that performing dual frequency saturation by alternating between positive and negative frequency irradiation on a timescale τ_{switch} introduces a T_{1D} dependence to the measured ihMT signal(37). This can be achieved by adjusting the time between pulses, Δt, or by keeping Δt constant but applying a number of pulses at the same frequency before switching (Fig. 4).

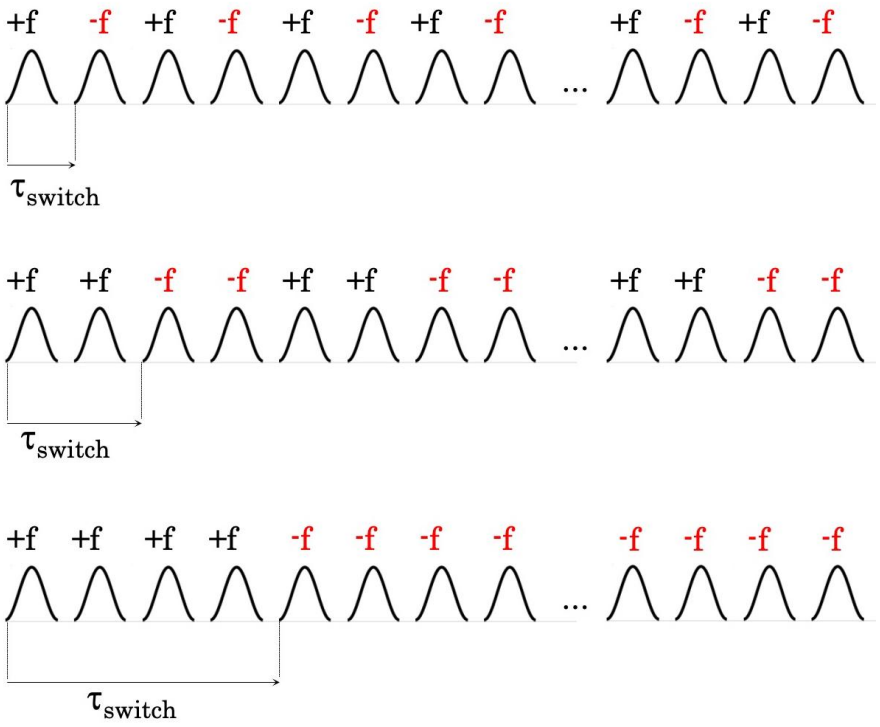

Figure 4. Dual offset saturation achieved with frequency-alternated pulses on a timescale of τ_{switch}. Increase of τ_{switch} introduces a dependence of the resulting ihMT signal on T_{1D} relaxation.

T_{1D} can be estimated by fitting a theoretical biophysical ihMT model to the decay of ihMT signals acquired with different τ_{switch}s. A single non-zero T_{1D} compartment model was initially used with this modified sequence to estimate the value of T_{1D} *in vivo* in human brain white matter(T_{1D} varying between 5.8 and 6.6 ms depending on region and analysis method) and gray matter (T_{1D} of 6.0 ms) (37) and in mouse head (T_{1D}=*6.1±0.8 ms* in internal capsule white matter (WM), T_{1D}=*5.6±1.2 ms* in cortical gray matter (GM), and T_{1D} = 2.2 ± 0.6 ms in muscle) (28). Importantly, both these studies focused on fitting the ihMT difference signal without attempting to fit the MT data with a complete

model as in reference (2) where simultaneous fitting of MT data suggested a short T_{1D} pool was required. Since only the longest T_{1D} molecules contribute substantially to ihMT at lower powers (eq. [9] and (38)), the use of higher saturation powers is likely necessary to observe the contribution of other shorter T_{1D} components in the ihMT difference signal.

A detailed study of fixed rat spinal cord ihMT performed at 40°C has shown that two non-zero T_{1D} components are required to properly interpret the ihMT signal decay with the modified ihMT sequence at high RF saturation power(38). Estimated values were in the hundreds of microseconds range (T_{1D}*~500 µs* for WM and *~400 µs* for GM) for the short component and in the millisecond range (T_{1D}*~10 ms* for WM and *~8.5 ms* for GM) for the long one. The existence of multiple T_{1D}s in the complex biological structures that make up the WM and GM of the central nervous system (e.g., myelin membrane) is not surprising as various populations of protons and motions should be involved. This is moreover in line with NMR experiments performed on lipid systems made of multilamellar vesicles that mimic the lipid composition of myelin and lamellar lipid bilayers (PL161), which show that the dipolar decay time dependence of the Jeener-Broekaert echoes is multi-exponential, and hence shows the existence of multiple T_{1D}s in lipid membranes(20,38).

These observations raise several major challenges to exploiting T_{1D} contrast as a novel biomarker of myelin membrane: what is the validity of T_{1D} values estimated by ihMT? How do we interpret the multiple T_{1D} values in terms of intra, intermolecular and collective motions in membranes? How do we isolate the contribution of different T_{1D}s within the ihMT signal and use them as informative contrasts?

Undoubtedly, combining ihMT MRI with liquid-state and solid-state NMR would be an interesting way to start tackling the first two challenges. Under similar experimental conditions (e.g., magnetic field strength, temperature), T_{1D} values estimated by ihMT MRI in various *in vitro* and *ex vivo* lipid system samples could be validated against reference values measured by Jeener-Broekaert NMR. Such investigations will offer the possibility to explore high RF power levels that are not accessible *in vivo* due to SAR constraints, and hence the sensitization to relatively short T_{1D} values(12). Note, however, that the modified ihMT sequence inherently biases T_{1D} estimation to values longer than the shortest switching time (τ_{switch}) with which data were acquired. Therefore, this limited range of accessible T_{1D} values should be considered when using ihMT compared to Jeener-Broekaert NMR. The association of T_{1D} values with peculiar motions will require NMR analyses probing lipid membrane phases and dynamics (e.g., ^{2}H spectrum second moment analyses(39,40)) combined with the theory of dipolar relaxation(41–43).

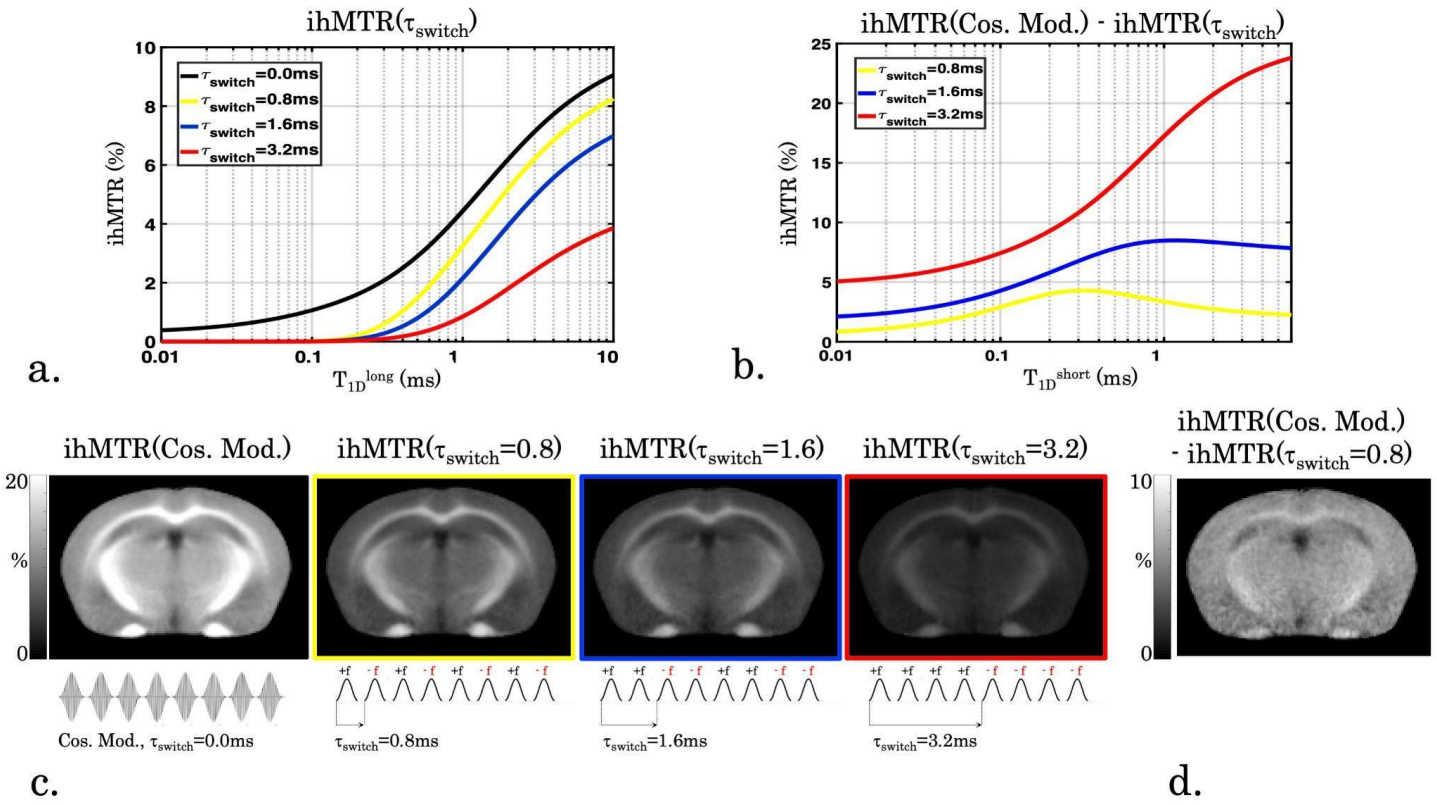

Figure 5. T_{1D} filtering effects achieved in images of the mouse brain by varying τ_{switch}.(44) (a) Simulations of ihMTR as a function of T_{1D} for different τ_{switch} values shows the preferential attenuation of shorter T_{1D} signals with increasing τ_{switch} , effectively creating a high-pass T_{1D} filter. (b) Simulated result from the difference between ihMTRs at two different τ_{switch} times, cosine modulated (effectively τ_{switch}=0) and a nonzero value. This effectively creates a bandpass filter for T_{1D}. These simulations assume a 2 T_{1D}-component (short, T_{1D}^{short} and long, T_{1D}^{long}) tissue model with relative pool sizes of short and long T_{1D} pools of 0.75/0.25. In (a), the value of T_{1D}^{short} was set to just infinitesimally above 0 ms. In (b), T_{1D}^{long} was set to 6 ms. (c) In-vivo mouse ihMTR brain images acquired with different τ_{switch} times. Note the greater gray-white matter contrast with longer τ_{switch}s. (d) A bandpass ihMTR image created by subtracting the cosine modulated and τ_{switch}=0.8 ms images of (c). Adapted from (44).

In vivo imaging of long and short T_{1D} components separately can be achieved with ihMT, when using a strategy based on so-called T_{1D}-filtering(45). The T_{1D}-filtering principle relies on the sensitivity of ihMT to T_{1D} when using frequency-alternated pulses with different switching times, τ_{switch}, for the dual-offset saturation experiment (Fig. 4), and has been recently characterized(44). The lengthening of τ_{switch} efficiently attenuates the signal associated with T_{1D} values shorter than τ_{switch} (even eliminates their contribution when $T_{1D} << \tau_{switch}$) thereby generating an ihMT high-pass T_{1D}-filter with increasing cutoff values (Fig. 5a) . IhMT high-pass T_{1D}-filters with high cutoff values can selectively image longer T_{1D} contributors and increase the WM/GM contrast (Fig. 5c). Isolation of short T_{1D} components is

possible by combining different T_{1D} filters. Hence, the subtraction between ihMT signals acquired with a zero T_{1D} cutoff (i.e, τ_{switch}=0ms, achieved by the use of cosine-modulated pulses for the dual offset saturation) and a non-null τ_{switch} configuration (e.g, τ_{switch} =0.8 ms) creates a bandpass T_{1D} filter, which isolates short T_{1D} components, approximately within the 100 µs to 1 ms range (Figs. 5b,d). These results were obtained in preclinical studies performed on mice using high saturation RF power (B_{1RMS}= 6.7 µT). The possibility to isolate short T_{1D} components with RF power values equivalent to those used in clinical studies (e.g. B_{1RMS} on the order of 3 µT at 3T) remains an open challenge. Bandpass ihMT T_{1D} filters created by the subtraction of τ_{switch}=0 ms and τ_{switch}=0.8 ms, also suffer from low SNR. More optimized linear combinations of T_{1D} filters with different cutoffs could be considered to create more flexible and sensitivity enhanced bandpass T_{1D} filters.

3. Optimizing acquisition methods

The ihMT signal is obtained from at least two separate MT experiments with different off-resonance saturation. Conceptually, we can divide the experiments into MT preparations and image acquisitions, though the two may be rapidly interleaved in time in some sequences.

The choice of preparation pulses is crucial for the ihMT effect. ihMT can be implemented either with relatively long (5 ms or longer) RF pulses or with a series of shorter shaped pulses. Dual frequency irradiation for longer pulses is achieved by cosine modulation(1), which effectively provides simultaneous irradiation at both frequencies (dual-band) (Figure 6B left). More complex modulation functions have even been used to combine MT saturation and water excitation in gradient echo sequences(46). When a series of shorter pulses are used, successive alternation of the frequency of the pulses between negative and positive frequency values can instead be employed (Figure 6B right) (1,37). As discussed above, this will lead to additional T_{1D} weighting of the ihMT images(45) and adds the option of switching frequency less often, e.g. every two pulses, to further increase T_{1D} weighting(37,45). When short pulses are used, care must be taken to avoid direct saturation of the water line because of the broad bandwidth of these pulses(47). Shaping of the pulses, typically with Hann or Tukey windows, to minimize the bandwidth is essential. When the preparation pulses need to be applied at high power, both the cosine modulation and the shaping of shorter pulses require higher peak RF amplitude than an unmodulated longer pulse. Hardware limits on the available peak RF amplitude can become a limiting factor for sequence optimization in some circumstances such as when power is applied at a low duty cycle.

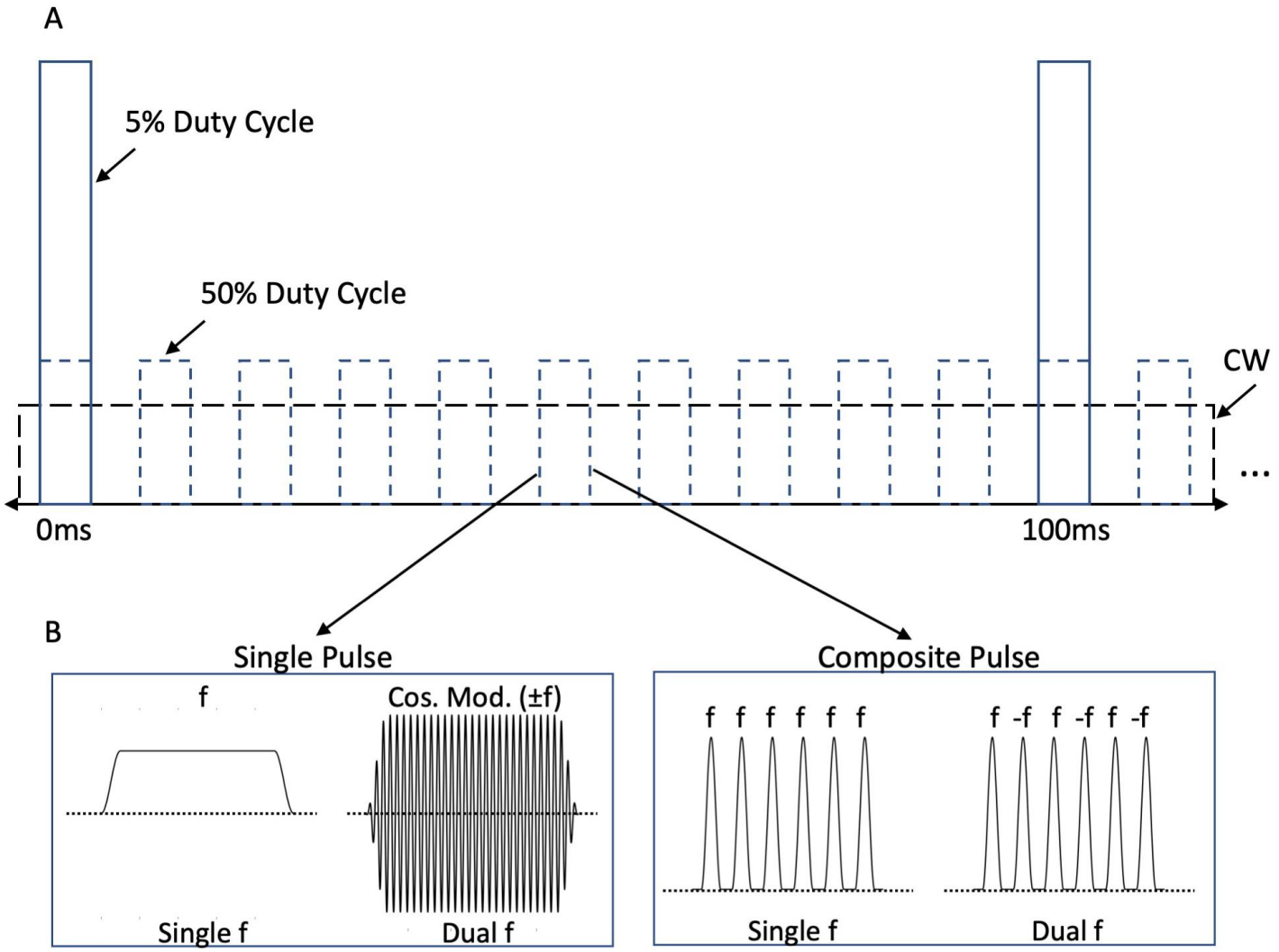

Figure 6. Off-resonance Saturation at Different Duty Cycles. (A) Relative timing and amplitude of irradiation continuously (CW), at 50% (high) duty cycle, and at 5% (low) duty cycle. Note the much larger pulse amplitudes when 5% duty cycle saturation is applied at equal time averaged power. The pulses are shown as rectangular to simplify the figure but are detailed in (B). Pulses may be either single pulses that are cosine modulated for dual frequency saturation, or a composite of several pulses where dual frequency saturation is achieved by frequency alternation.

The duty cycle of saturation is another key choice in sequence design. As indicated by equation [9], ihMT increases very rapidly with applied power, approximately ω_1^4. Though this solution was derived for the steady state, it can still provide intuition for duty cycle effects since it has been shown that pulsed MT effects can be approximated by using the time average of the RF saturation rate in the steady state equation(48). The single frequency RF saturation rate with dipolar order effects rapidly approaches the steady state expression in eq. [6] on a timescale of T_{1D} so substituting a time average of eq. [6] for pulses comparable to or longer than T_{1D} is also approximately correct for ihMT. When a brief group of one or more pulses is applied infrequently but at high RF amplitude (low duty cycle)

(Figure 6), the time average of ω_1^4 is larger than when the same pulses are applied more frequently but at lower RF amplitude (high duty cycle) to match time averaged RF power (ω_1^2). Much greater ihMT effect is realized with such a low duty cycle application as has been shown with full numerical solution of the coupled equations and experimentally(24,25). In line with these considerations, it was found that various RF duty cycle conditions lead to different RF power dependence of the ihMT signal(24). In most in-vivo imaging applications, remaining within safety guidelines for applied power sets a limit on the time averaged RF power. Since the ihMT increase with reduced duty cycle can be very large, greater than threefold, the use of low duty cycle preparations to achieve higher signal and signal-to-noise ratio is becoming increasingly preferred. With high RF saturation power, which is typically the case for low duty cycle experiments, the signal contribution from shorter T_{1D} molecules can become substantial(38,44,49,50), opening the possibility to image other molecular structures and tissues than myelin(51,52). The increased sensitivity to short T_{1D}s does reduce the specificity of the ihMT signal to myelin, however. This decreased specificity can be compensated by adding T_{1D} filtering through slower frequency alternation(49).

Many potential imaging sequences can be used for acquisition of ihMT data. Early implementations of ihMT concentrated on demonstration of the ihMT phenomenon using longer preparations before rapid, single-shot acquisitions. For imaging purposes, this was achieved with both single-shot fast spin-echo (ssFSE)(1,22) and echo-planar-imaging(2) (EPI) readouts. ssFSE has reduced vulnerability to magnetic field nonuniformity related signal loss and geometric distortion. This sequence is particularly appealing for studies in the spinal cord and outside the CNS where the magnetic field is less uniform. An ssFSE sequence was combined with a binning technique to compensate for physiological motion and provide better delineation of the spinal cord in ihMT MRI(53). EPI provides faster acquisition of multiple slices, especially with newer multiband acceleration methods. Since T_2 decay of the signal is an undesirable source of signal loss, the TE of both EPI and ssFSE should be minimized, potentially with partial Fourier and/or centric phase encode ordering.

3D acquisition of ihMT can potentially provide greater spatial coverage, image quality, and speed than 2D acquisitions. Steady state 3D gradient echo acquisitions have long been used for MT studies of the brain(54) and were a natural approach to 3D ihMT. In this approach, short preparation pulses are interleaved with a readout for an approximate steady-state(30,55). Measurements of ihMT with this approach were similar to earlier results with 2D techniques despite the much shorter echo time of the gradient echo sequence. Though the myelin specific ihMT signal is likely more coupled to shorter T2 myelin water trapped in the myelin sheath, previous studies have found that longitudinal

magnetization exchange between the myelin water and non-myelin water occurs on a timescale of a few 100 ms which is sufficiently fast that much of the ihMT signal will be in the non-myelin water(56). This was further confirmed in a multi gradient echo sequence that showed similar ihMT for echoes spaced several milliseconds apart(57). This multi-echo sequence was used to remove adipose fat signal using the Dixon approach. Though adipose tissue shows negligible ihMT effect, its brightness and partial volume in ihMT acquisitions can be a source of artifacts and error.

Steady state 3D methods can be modified to acquire multiple lines of k-space during the readout after each preparation pulse to increase image acquisition speed. This is particularly desirable when low duty cycle acquisitions are performed by using a longer TR between MT pulses. Using this approach, Mchinda et al.(24) showed that TRs in excess of 50 to hundreds of ms, depending on RF saturation conditions, provided the greatest ihMT signal. To control the average RF power, they also reduced the MT pulse amplitude towards the edge of k-space. More recently, Wood et al.(58) implemented a similar sequence using a silent RUFIS sequence, enabling ihMT acquisition without perceived acoustic noise. These multiple k-space excitation sequences blur the conceptual boundary between steady state sequences and prepared sequences. As with prepared sequences, modulation of echo amplitude across the burst of readouts can introduce blurring or other artifacts.

Fully prepared 3D sequences offer potential benefits in flexibility of saturation timing and control of power deposition. In these sequences, the preparation and TR are long compared to the repetition time of MT saturation pulses and comparable to T_1. An ihMT Magnetization Prepared RApid Gradient Echo (MPRAGE) sequence has been reported(59) that employed 1 second of saturation and a TR of 2 s. A long train of gradient echoes speeds the acquisition. Whole brain imaging of ihMT can be achieved in a clinically feasible scan time. Spatial resolution as high as 1.6 mm isotropic has been achieved, enabling detailed characterization of cortical gray matter ihMT(60). Improved sensitivity of prepared 3D acquisition may be possible with refocused sequences such as FSE or balanced SSFP. Recent work with FSE sequences supports the higher signal-to-noise ratio with refocused acquisitions, but control of added noise from CSF motion may require FLAIR or other techniques(61).

ihMT acquisitions can be performed across a wide range of field strengths. The lineshapes and widths of dipolar broadened lines are largely insensitive to field strength. At high field, the higher intrinsic sensitivity of imaging must compete with restrictions on deposited RF power that reduce the ihMT signal. While high field ihMT has been reported in small animals up to 11.75T(45), translation to human imaging at 7T and beyond is still under development. Acquisitions at low field strength are still

quite competitive because higher RF amplitudes and powers can be employed. In-vivo acquisition in humans have been reported at 0.5T(62) and ihMT in specimens has been studied at fields as low as 1.5mT(63).

4. Optimizing quantification methods

An important goal for ihMT development is to achieve a reproducible quantitative measure of tissue. Considerable work remains after image acquisition to extract quantitative parameters. First, preprocessing of images to address motion and noise is desirable(e.g. (64)). Then derivation of a quantitative metric must be performed. ihMTR (eq [1]) has been used as a metric in most of the early literature. As has previously been found for MTR(65), this metric includes factors related to the sequence design, tissue T_1 relaxation and other model parameters (Eq. [4]) and the spatially varying RF magnetic field amplitude that renders it less reproducible, tissue specific, and generalizable than would be ideal. A recent study(47) has shown, however, that it is possible to strongly attenuate the sensitivity of ihMTR to B_1 inhomogeneities using specific RF saturation conditions consisting of particularly low RF duty cycle.

Two related metrics that are an alternative to ihMTR have been proposed as potentially more independent of T_1, RF magnetic field and sequence parameters. The first metric(25,66) is an inverse subtraction of ihMT as in eq. [9], an approach that has been advocated for related purposes in the MT(67) and CEST(68) literature. In its simplest form, one defines ihMTRinv as

$$ihMTR_{inv} = S_0\left(\frac{2}{S_{dual}} - \frac{1}{S_{pos}} - \frac{1}{S_{neg}}\right) \quad . \qquad [11]$$

Where S_{pos}, S_{neg} and S_{dual} correspond to the MR signal obtained after single positive, single negative and dual offsets saturation respectively. As will be described shortly, ihMTRinv is particularly appropriate in steady state sequences. A second metric, ihMTsat, is a generalization of the MTsat approach(67). The MTsat approach assumes that MT is achieved with relatively brief RF pulses or pulse trains repeated with a period that is long compared to the exchange time between the bound and free pools. The effect of an MT saturation pulse can then be approximated as an attenuation of the longitudinal magnetization of the free pool by a factor $(1-\delta)$ where δ is the MTsat metric. An analogous ihMTsat metric was defined(60) as

$$ihMTsat = 2\delta_{dual} - \delta_{pos} - \delta_{neg}$$ [12]

Whatever sequence is employed, one can infer δ by inversion of the signal equations, either by analytical or numerical solution. For example, consider the steady state gradient echo sequence with a saturation pulse applied shortly before a readout flip angle, α. Under the assumption of a small flip angle, small δ, and TR << T_1, the steady state signal equation is given by

$$S \approx GM_0 \frac{\alpha}{\left(1 + \frac{\left(\frac{\alpha^2}{2} + \delta\right)T_1}{TR}\right)},$$ [13]

where G is an imaging gain factor. From three experiments, typically two reference experiments without MT pulses but differing α and/or TR and a third experiment with MT, the quantities (G M0), δ, and T_1 may be determined. The inverse ihMTR is then closely related to the ihMTsat:

$$ihMTR_{inv} = S_0\left(\frac{2}{S_{dual}} - \frac{1}{S_{pos}} - \frac{1}{S_{neg}}\right) = \frac{\alpha}{1 + \frac{\alpha^2 T_1}{2TR}}\left(\frac{\left(2\delta_{dual} - \delta_{pos} - \delta_{neg}\right)T_1}{\alpha TR}\right) = ihMTsat\left(\frac{T_1}{TR + \frac{\alpha^2 T_1}{2}}\right).$$

[14]

It is convenient to use a larger flip angle, *c α*, to acquire the ihMT reference image, S_{lf}. a. If this flip angle is large enough such that

$$\frac{\left(\frac{c^2\alpha^2}{2}\right)T_1}{TR} >> 1,$$ [15]

then using this larger flip angle reference enables calculating ihMTsat,

$$ihMTsat = \left(\frac{c\alpha^2}{2}\right)ihMTR_{invlf} = \left(\frac{c\alpha^2}{2}\right)S_{lf}\left(\frac{2}{S_{dual}} - \frac{1}{S_{pos}} - \frac{1}{S_{neg}}\right).$$ [16]

If the difference of deltas depends on the RF amplitude squared, then ihMTsat calculated this way is independent of variations of RF field and calibration(66). A related semi-quantitative metric of ihMT saturation rate referred to as qihMT has been defined(30) and used in a number of studies(30,69–72).

$$qihMT = \left(\frac{c\alpha_{nom}^2}{4TR} \right) ihMTR_{invlf} . \qquad [17]$$

Where the flip angle is the nominal, or targeted, flip angle and not the actual flip angle due to spatial variation or miscalibration of the RF field. Since qMT is used to describe the quantitative measurement of potentially many MT model parameters(65), the use of the name qihMT for this metric needs to be reconsidered. When the RF pulse power is in the appropriate range, then the ihMT effect is approximately proportional to the RF amplitude squared(25), and this metric is a simple T_1 and RF amplitude independent measure of ihMT effects. For in-vivo studies limited by RF safety guidelines, this power range occurs only when low duty cycle RF is applied. At higher duty cycle, quadratic RF correction of ihMT is insufficient to fully correct for RF amplitude dependence.

Though inverse subtraction metrics are appealing for their simplicity and the potential to acquire all information with one sequence type, there are potential sources of error that can be addressed with a more complete ihMTsat approach. These include the potential overestimation of T_1 with the reference images because of imperfect spoiling(73) and the size of the bound pool(74), the restriction to small flip angles, the need for steady state, and the possible need for more complex calibration functions to correct for RF amplitude dependence. Because methods for fast RF field mapping are increasingly available(75,76) and the RF field varies only slowly with position, measurement of the RF field is particularly appealing. In correcting for RF transmit field variations, it is important to note that MT without dipolar order effects, i.e. MT with dual frequency irradiation, has a different dependence on RF amplitude than the dipolar order effects responsible for ihMT(25). Thus, different calibrations are needed to correct them(60,77). Finally, it is worth noting that the ihMTsat framework generally relies on a relatively simple model for T_1 relaxation and, in particular, assumes a fast exchange limit between proton pools. A more comprehensive model (e.g. involving more compartments(78,79)) may be required to properly account for T_1 relaxation effects in biological tissues.

Measures like ihMTsat provide robustness to experimental parameters and imperfections but they depend on the RF pulse shapes, frequencies, and amplitudes employed and are not direct

measurements of tissue model parameters. Investigators have pursued such direct measurements of MT models using methods known as qMT(65). These methods have the potential to measure fractional pool sizes, T_{1D}, exchange rates, and lineshapes. Recent work using MR fingerprinting methods has reported the use of qMT type analysis on ihMT data(80). More such studies are needed to better characterize the tissue parameters in-vivo and to guide the physiologic interpretation of any changes in ihMT measures with pathology.

5. Validating ihMT measures

A key step in acceptance and understanding of ihMT imaging is the comparison and validation of its measures against gold standard or accepted measures. As ihMT involves NMR specific quantities, some aspects can only be compared to other NMR acquisitions. The comparison of T_{1D} measures between Jeener-Broekaert and ihMT approaches, as suggested earlier, is one such comparison. In performing such measures, careful attention to tissue temperature is essential. Since Jeener-Broekart can only be performed on small tissue samples, further study of the effect of fixation on tissue ihMT related measures is merited. A second form of validation is comparing ihMT measures that are proposed markers for tissue content or structure with other methods, both ex-vivo and in-vivo.

Because ihMT is particularly sensitive to the long T_{1D}s observed in myelinated tissues, validation of ihMT as a marker of myelin is an important step. One challenge of validating measures is that myelin is a complex structure containing multiple lipids and proteins(81) that also traps water in thin layers. Though all these constituents should be correlated with myelin, they may vary differently with myelin age, thickness, lipid content, and especially pathology.

The sensitivity and the specificity of ihMT for myelin was first validated histologically in a comparative study with fluorescence microscopy performed on genetically modified PLP-GFP (proteolipid protein-Green Fluorescent Protein) mice. PLP-GFP is the animal model in which the green fluorescent protein (GFP) is specifically expressed in myelinating oligodendrocytes(82,83). In these mice, the GFP fluorescence, which is directly observable and quantifiable with fluorescence microscopy, thus reflects the expression of proteolipid protein, the major myelin protein in the central nervous system and represents a direct and very valuable tool to observe and quantify myelin content. Correlation analyses between ihMT signal and GFP signal measured in different brain structures demonstrated strong association of ihMT with myelin content and furthermore highlighted the influence of T_{1D}-filtering in the sensitivity and the specificity of ihMT techniques(49), Figure 7. Another work compared

ihMT measures with Myelin Basic Protein (MBP) staining and another MRI myelin measure, Myelin Water Fraction (MWF) in fixed tissue(21). Again, T_{1D} filtered ihMT showed greater specificity to white matter than unfiltered, high power ihMT at body temperatures. Comparison to MWF was complicated by poor sensitivity to MWF at body temperature and poor sensitivity to filtered ihMT at room temperature. However, the low temperature dependence of high power, unfiltered ihMT allowed comparison with MWF at room temperature and they were well correlated. A more recent work further demonstrated that ihMT T_{1D} filters highly weighted toward long T_{1D} values provide the highest specificity to myelination. Conversely, the low specificity of ihMT bandpass T_{1D} filter ($100us<T_{1D}<1ms$) indicates that the short T_{1D} components of the ihMT signal are mostly associated with non-myelin protons(50). Further characterization of the sources of these shorter T_{1D} components is needed.

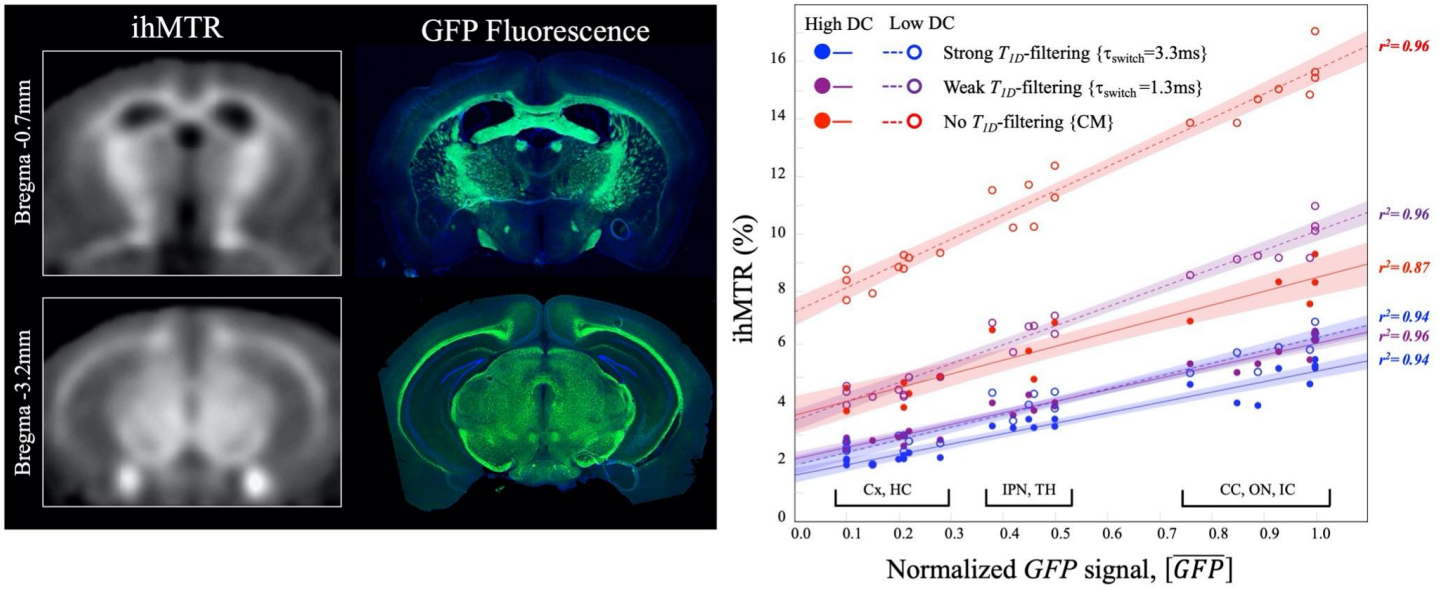

Figure 7. A validation study correlating ihMTR with green fluorescence protein (GFP) signal reflecting proteolipid protein gene expression, a myelin marker. Regional signal on ihMTR and GFP images, left, was measured in different white and gray matter areas - internal capsule (IC), corpus callosum (CC), optic nerves (ON), thalamus (Th), cortex (Cx), hippocampus (HC) and Inter-Peduncular Nucleus (IPN)- and then a linear regression with GFP as the dependent variable was performed. ihMTR was measured for low and high duty cycles (DC) and T_{1D} filters, characterized by the τ_{switch} value. Higher ratios of slope to intercept, corresponding to higher specificity to myelin, were observed with stronger T_{1D} filtering. Adapted from (49).

In human studies, validation has primarily taken the form of comparison between potentially myelin specific MRI measures. One study compared high duty cycle 3D gradient echo ihMT with diffusion MRI metrics and mcDESPOT measures of MWF in a cohort of healthy children(30). Correlation

between radial diffusion and other metrics was modest. ihMT correlated reasonably well with the MWF measure in white matter, but not in gray matter. However, after the study, others have raised questions about biases in mcDESPOT fitting algorithms, (84). Another study(23) compared high duty cycle gradient echo ihMT with a multi-echo MWF acquisition and diffusion metrics in healthy adults. ihMT correlated well with the MWF measure but correlations with fractional anisotropy and radial diffusivity were modest. In both these studies, it was noted that there was a relationship between ihMT and the angle between the main magnetic field and the direction of the tract, as measured by the principal axis of the diffusion tensor. This may represent a combination of the angular dependence of dipolar order effects, as discussed above, and the higher myelination of major ascending tracts in the brain. Experimental methods for direct measurement of angular dependence effects in ihMT have been proposed that can differentiate these factors(31). A further test of the myelin specificity of ihMT studied the variation of ihMT in gray matter across different cortical regions. This study(60) with low duty cycle MPRAGE acquisition demonstrated similar spatial dependence to reports using the ratio of T_1 and T_2 weighted images and some histological studies.

Clearly more extensive validation studies are needed to fully understand the sensitivity of ihMT to specific tissue types and especially pathology. Since signal-to-noise, T_{1D} filtering and myelin specificity are all functions of sequence choices and quantification methods, agreement on standardized methods for further validation and application should be a priority.

6. Disseminating standard methods and evaluating them in different pathologies.

Distribution and standardization of pulse sequence implementations for ihMT are still at an early phase. Part of the problem is the rapid pace of increase in understanding of ihMT properties, such as the existence of multiple T_{1D} compartments in tissue(38). Another issue is the improvement in image acquisition, especially with low duty cycle, high peak power implementations(24,25). Despite these challenges, imaging methods for ihMT are approaching a default imaging protocol that has

1. Low duty cycle, high peak power RF saturation for high signal and SNR(24,25).
2. 3D gradient echo readout with acquisition of multiple k-space lines after the preparation.
3. Field strength of either 3.0 or 1.5 Tesla for human studies, though ihMT is not very sensitive to field strength, and likely a field greater than or equal to 7T for preclinical studies, where RF power concerns are reduced and SNR higher, is advantageous.

Example ihMTsat images achieved with a protocol meeting these guidelines: an ihMT prepared MPRAGE gradient echo sequence and low duty cycle saturation, are shown in Figure 8.

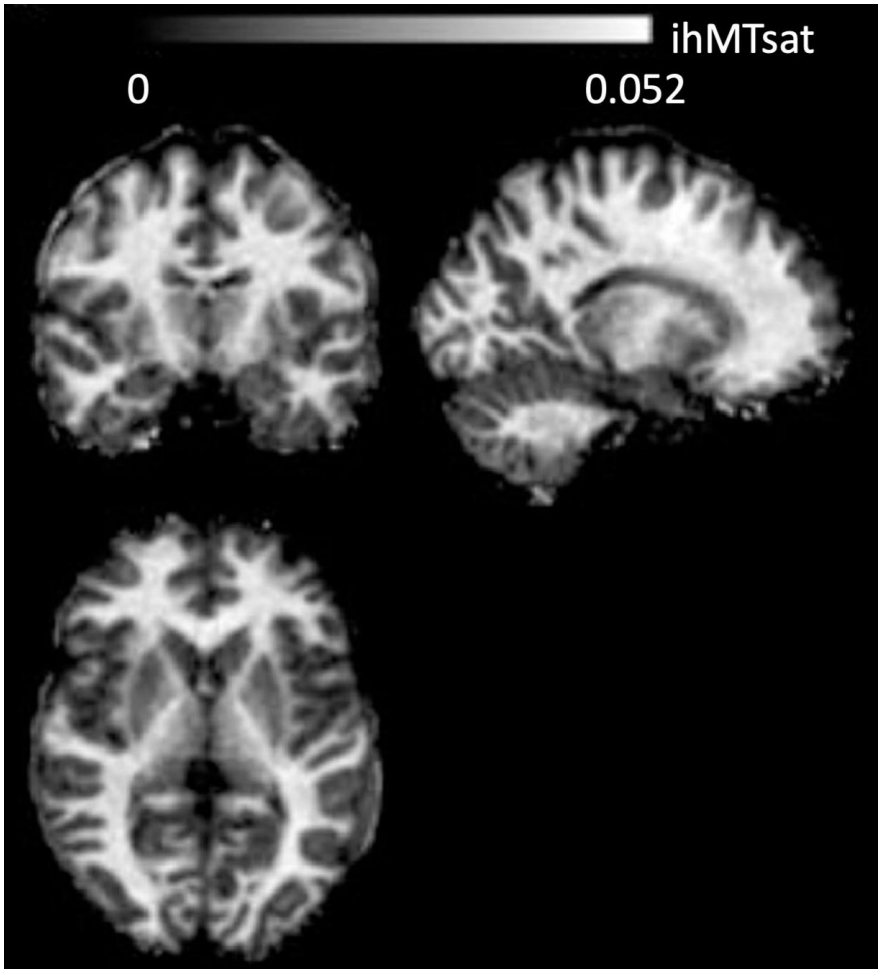

Figure 8. Example volumetric imaging ihMTsat results from a healthy volunteer at 3T. A magnetization prepared 3D sequence acquired images at 1.6 mm cubic resolution. Low duty cycle saturation (5%, RF pulse peak B_1 of 14 μT) and cosine modulated pulses for dual saturation were employed. ihMTsat quantification included correction for B_1 inhomogeneity using a separately acquired map. Adapted from (60).

Specific characteristics of acquisition and quantification still being debated and developed include

1. Whether T_{1D} filtering(45) with frequency alternation(37) should be employed for greater T_{1D} specificity or cosine modulated pulses for greater ihMT signal.
2. Whether an ihMT prepared MPRAGE(59) or hybrid steady state gradient echo sequence(24) should be used.
3. Whether ihMTR or more advanced measures such as ihMTsat(60,67) or a model based approach(65) should be used for quantification.

4. What methods should be used to correct for transmit field variations and T_1 effects on measures of ihMT(47,60,80).

Initial applications of ihMT to the study of neurological conditions have been promising. All evaluations in pathology published to date have employed high duty cycle ihMT, so the improvement in patient image quality and change in disease sensitivity with low duty cycle acquisitions has yet to be described. Two groups have reported sensitivity to white matter changes in Multiple Sclerosis (MS) brain. One(85) employed a 2D sequence and ihMTR quantification and found higher effect sizes in normal appearing white matter (NAWM) and higher correlations with disability score than for MT. A second(70) employed a 3D steady state sequence and the qihMT metric described above and again found a greater effect size of MS changes with ihMT than MT. This group also separately evaluated test-retest reproducibility in a cohort of healthy adults(69). MS effects in the spinal cord have also been probed with ihMT(86). There, ihMT decreases are pronounced and strongly correlated with disability. Additionally, ihMT in the spinal cord was found to correlate with age in healthy subjects(87). ihMT was also shown to be highly sensitive to spinal cord changes in amyotrophic lateral sclerosis(88). Interestingly, two studies(71,72) have demonstrated myelin changes in the brains of patients with major depression, suggesting a role for ihMT to complement diffusion imaging in studies of white matter pathology associated with psychiatric disorders.

Conclusion

ihMT offers a unique view on the physical state of motionally constrained molecules through its sensitivity to T_{1D}. Because some molecules in myelin, presumably membrane lipids, have longer T_{1D}s than most bound molecules in other tissues, ihMT is particularly attractive for characterizing myelin, but emerging methods to quantify shorter T_{1D} pools point to the potential for other applications. As described above, great progress has already been made in defining the physics underlying ihMT and developing acquisition and quantification methods. Initial validation studies and experience in clinical populations has also been reported. We have also detailed a number of challenges and future directions. We encourage a new generation of scientists to join us in exploring the full potential of ihMT.

References

1. Varma G, Duhamel G, de Bazelaire C, Alsop DC. Magnetization Transfer from Inhomogeneously

Broadened Lines: A Potential Marker for Myelin. Magn Reson Med. 2015 Feb;73(2):614–22.
2. Varma G, Girard OM, Prevost VH, Grant A, Duhamel GD, Alsop DC. Interpretation of magnetization transfer from inhomogeneously broadened lines (ihMT) in tissues as a dipolar order effect within motion restricted molecules. J Magn Reson. 2015 Nov;260:67–76.
3. Calucci L, Forte C. Proton longitudinal relaxation coupling in dynamically heterogeneous soft systems. Prog Nucl Magn Reson Spectrosc. 2009 Nov 1;55(4):296–323.
4. Wolff SD, Balaban RS. Magnetization transfer contrast (MTC) and tissue water proton relaxation in vivo. Magn Reson Med. 1989;10(1):135–44.
5. Liepinsh E, Otting G. Proton exchange rates from amino acid side chains— implications for image contrast. Magn Reson Med. 1996 Jan;35(1):30–42.
6. Wennerström H. Proton nuclear magnetic resonance lineshapes in lamellar liquid crystals. Chem Phys Lett. 1973 Jan 1;18(1):41–4.
7. Morrison C, Henkelman RM. A model for magnetization transfer in tissues. Magn Reson Med. 1995;33(4):475–82.
8. Bloom M, Burnell EE, Roeder SBW, Valic MI. Nuclear magnetic resonance line shapes in lyotropic liquid crystals and related systems. J Chem Phys. 1977;66:3012.
9. Goldman M. Spin Temperature and Nuclear Magnetic Resonance in Solids. Oxford University Press. 1970.
10. Pake GE. Nuclear Resonance Absorption in Hydrated Crystals: Fine Structure of the Proton Line. J Chem Phys. 1948 Apr;16(4):327–36.
11. Bloembergen N. Spin Relaxation Processes in a Two-Proton System. Phys Rev. 1956 Dec 15;104(6):1542–7.
12. Manning AP, Chang KL, MacKay AL, Michal CA. The physical mechanism of “inhomogeneous” magnetization transfer MRI. J Magn Reson. 2016 Nov 24;274:125–36.
13. Yang H, Schleich T. Incorporation of Dipolar Order Effects into the Three Component Proton Cross Relaxation Magnetization Transfer Formalism. In: Proceedings of the SMRM. New York, New York USA; 1993. p. 1286.
14. Yeung HN, Adler RS, Swanson SD. Transient Decay of Longitudinal Magnetization in Heterogeneous Spin Systems under Selective Saturation. IV. Reformulation of the Spin-Bath-Model Equations by the Redfield-Provotorov Theory. J Magn Reson A. 1994 Jan;106(1):37–45.
15. Morrison C, Stanisz G, Henkelman RM. Modeling magnetization transfer for biological-like systems using a semi-solid pool with a super-Lorentzian lineshape and dipolar reservoir. J Magn Reson B. 1995 Aug;108(2):103–13.
16. Danek AN, Bryant RG. Decay of Dipolar Order in Diamagnetic and Paramagnetic Proteins and Protein Gels. J Magn Reson. 2000 Mar;143(1):35–8.
17. Sled JG, Pike GB. Quantitative Interpretation of Magnetization Transfer in Spoiled Gradient Echo MRI Sequences. J Magn Reson. 2000 Jul;145(1):24–36.
18. Alsop DC, de Bazelaire C, Duhamel G. In-vivo Imaging of an Inhomogeneous Component of Magnetization Transfer in Human White Matter. In: Proceedings of the ISMRM. Kyoto, Japan; 2004. p. 2324.
19. Lee JS, Khitrin AK, Regatte RR, Jerschow A. Uniform saturation of a strongly coupled spin system by two-frequency irradiation. J Chem Phys. 2011;134(23):234504.
20. Swanson SD, Malyarenko DI, Fabiilli ML, Welsh RC, Nielsen JF, Srinivasan A. Molecular, dynamic, and structural origin of inhomogeneous magnetization transfer in lipid membranes. Magn Reson Med. 2017 Mar;77(3):1318–28.
21. Prevost VH, Yung A, Morris SR, Vavasour IM, Samadi-Bahrami Z, Moore GRW, et al. Temperature dependence and histological correlation of inhomogeneous magnetization transfer and myelin water imaging in ex vivo brain. NeuroImage. 2021 Aug;236:118046.
22. Girard OM, Prevost VH, Varma G, Cozzone PJ, Alsop DC, Duhamel G. Magnetization transfer from inhomogeneously broadened lines (ihMT): Experimental optimization of saturation parameters for human brain imaging at 1.5 Tesla. Magn Reson Med. 2015 juin;73(6):2111–21.
23. Ercan E, Varma G, Mädler B, Dimitrov IE, Pinho MC, Xi Y, et al. Microstructural correlates of 3D steady-state inhomogeneous magnetization transfer (ihMT) in the human brain white matter assessed by myelin water imaging and diffusion tensor imaging. Magn Reson Med. 2018 Dec;80(6):2402–14.
24. Mchinda S, Varma G, Prevost VH, Le Troter A, Rapacchi S, Guye M, et al. Whole brain inhomogeneous magnetization transfer (ihMT) imaging: Sensitivity enhancement within a steady-state gradient echo sequence. Magn Reson Med. 2018 May;79(5):2607–19.

25. Varma G, Girard OM, Mchinda S, Prevost VH, Grant AK, Duhamel G, et al. Low duty-cycle pulsed irradiation reduces magnetization transfer and increases the inhomogeneous magnetization transfer effect. J Magn Reson. 2018 Nov;296:60–71.
26. Portis AM. Electronic Structure of F Centers: Saturation of the Electron Spin Resonance. Phys Rev. 1953 Sep 1;91(5):1071–8.
27. Maricq MM, Waugh JS. NMR in rotating solids. J Chem Phys. 1979;70(7):3300.
28. Prevost VH, Girard OM, Varma G, Alsop DC, Duhamel G. Minimizing the effects of magnetization transfer asymmetry on inhomogeneous magnetization transfer (ihMT) at ultra-high magnetic field (11.75 T). Magn Reson Mater Phys Biol Med. 2016 Aug;29(4):699–709.
29. Provotorov BN. Theory of Double Magnetic Resonance in Solids. Phys Rev. 1962 Oct 1;128(1):75–6.
30. Geeraert BL, Lebel RM, Mah AC, Deoni SC, Alsop DC, Varma G, et al. A comparison of inhomogeneous magnetization transfer, myelin volume fraction, and diffusion tensor imaging measures in healthy children. NeuroImage. 2018 Nov 15;182:343–50.
31. Girard OM, Prevost VH, Mchinda S, Varma G, Alsop DC, Duhamel G. Anisotropy of inhomogeneous Magnetization Transfer (ihMT) in White Matter. In: Proceedings of the ISMRM. 2017. p. 472.
32. Pampel A, Müller DK, Anwander A, Marschner H, Möller HE. Orientation dependence of magnetization transfer parameters in human white matter. NeuroImage. 2015 Jul 1;114:136–46.
33. Morris SR, Frederick R, MacKay AL, Laule C, Michal CA. Orientation dependence of inhomogeneous magnetization transfer and dipolar order relaxation rate in phospholipid bilayers. J Magn Reson San Diego Calif 1997. 2022 May;338:107205.
34. Dufourc EJ, Mayer C, Stohrer J, Althoff G, Kothe G. Dynamics of phosphate head groups in biomembranes. Comprehensive analysis using phosphorus-31 nuclear magnetic resonance lineshape and relaxation time measurements. Biophys J. 1992 Jan;61(1):42–57.
35. Gaspar R, Andrew ER, Bryant DJ, Cashell EM. Dipolar relaxation and slow molecular motions in solid proteins. Chem Phys Lett. 1982 Feb 26;86(4):327–30.
36. Jeener J, Broekaert P. Nuclear magnetic resonance in solids: thermodynamic effects of a pair of rf pulses. Phys Rev. 1967;157(2):232.
37. Varma G, Girard OM, Prevost VH, Grant AK, Duhamel G, Alsop DC. In vivo measurement of a new source of contrast, the dipolar relaxation time, T1D , using a modified inhomogeneous magnetization transfer (ihMT) sequence. Magn Reson Med. 2017 Oct;78(4):1362–72.
38. Carvalho VND, Hertanu A, Grélard A, Mchinda S, Soustelle L, Loquet A, et al. MRI assessment of multiple dipolar relaxation time (T 1 D) components in biological tissues interpreted with a generalized inhomogeneous magnetization transfer (ihMT) model. J Magn Reson. 2020 Feb;311:106668.
39. Seelig J. Deuterium magnetic resonance: theory and application to lipid membranes. Q Rev Biophys. 1977 Aug;10(3):353–418.
40. Douliez JP, Léonard A, Dufourc EJ. Restatement of order parameters in biomembranes: calculation of C-C bond order parameters from C-D quadrupolar splittings. Biophys J. 1995 May;68(5):1727–39.
41. Van Steenwinkel R. The Spin Lattice Relaxation of the Nuclear Dipolar Energy in Some Organic Crystals with Slow Molecular Motions. Z Naturforsch. 1969;24a:1526–31.
42. Lauer O, Stehlik D, Hausser KH. Nuclear Zeeman and dipolar relaxation due to slow motion in aromatic single crystals. J Magn Reson 1969. 1972 Apr;6(4):524–32.
43. Ueda T, Takeda S, Nakamura N, Chihara H. Molecular Motion and Phase Changes in Long Chain Solid Normal Alkanes as Studied by ^{1}H and ^{13}C NMR. Bull Chem Soc Jpn. 1991 Apr;64(4):1299–304.
44. Hertanu A, Soustelle L, Le Troter A, Buron J, Le Priellec J, Carvalho VND, et al. T1D-weighted ihMT imaging. – Part I. Isolation of long- and short-T1D components by T1D- filtering. Magn Reson Med. 2022;In press 10.1002/mrm.29139.
45. Prevost VH, Girard OM, Mchinda S, Varma G, Alsop DC, Duhamel G. Optimization of inhomogeneous magnetization transfer (ihMT) MRI contrast for preclinical studies using dipolar relaxation time (T1D) filtering. NMR Biomed. 2017 Jun;30(6).
46. Malik SJ, Teixeira RPAG, West DJ, Wood TC, Hajnal JV. Steady-state imaging with inhomogeneous magnetization transfer contrast using multiband radiofrequency pulses. Magn Reson Med. 2020;83(3):935–49.
47. Soustelle L, Troalen T, Hertanu A, Mchinda S, Ranjeva JP, Guye M, et al. A strategy to reduce the sensitivity of inhomogeneous magnetization transfer (ihMT) imaging to radiofrequency transmit field variations at 3 T. Magn Reson Med. 2022;in press 10.1002/mrm.29055.

48. Ramani A, Dalton C, Miller D, Tofts PS, Barker GJ. Precise estimate of fundamental in-vivo MT parameters in human brain in clinically feasible times. Magn Reson Imaging [Internet]. 2002 Dec [cited 2022 Jun 6];20(10). Available from: https://pubmed.ncbi.nlm.nih.gov/12591568/
49. Duhamel G, Prevost VH, Cayre M, Hertanu A, Mchinda S, Carvalho VN, et al. Validating the sensitivity of inhomogeneous magnetization transfer (ihMT) MRI to myelin with fluorescence microscopy. NeuroImage. 2019 Oct;199:289–303.
50. Hertanu A, Soustelle L, Buron J, Le Priellec J, Cayre M, Le Troter A, et al. T1D-weighted ihMT imaging – Part II. Investigating the long- and short-T1D components correlation with myelin content. Comparison with R1 and the macromolecular proton fraction. Magn Reson Med. 2022;in press 10.1002/mrm.29140.
51. Varma, Gopal, Callahan, Cody, Girard, Olivier M., Duhamel, Guillaume, Grant, Aaron K., Alsop, David C. In vivo inhomogeneous magnetization transfer (ihMT) outside the brain using radial ultra-short echo-time acquisitions. In: Proceedings of the ISMRM. 2019. p. 4912.
52. Varma G, Coutinho de Souza, P., Prevost, V., Girard, O., Carvalho, V., Mchinda, S., et al. Towards short dipolar relaxation time, T1D, MRI. In: Proceedings of ISMRM. 2018. p. 787.
53. Girard OM, Callot V, Prevost VH, Robert B, Taso M, Ribeiro G, et al. Magnetization transfer from inhomogeneously broadened lines (ihMT): Improved imaging strategy for spinal cord applications. Magn Reson Med. 2017;77(2):581–91.
54. Dousset V, Grossman RI, Ramer KN, Schnall MD, Young LH, Gonzalez-Scarano F, et al. Experimental allergic encephalomyelitis and multiple sclerosis: lesion characterization with magnetization transfer imaging. Radiology. 1992 Feb;182(2):483–91.
55. Varma G, Schlaug G, Alsop DC. 3D Acquisition of the Inhomogeneous Magnetization Transfer Effect for Greater White Matter Contrast. In: Proceedings of the ISMRM. Salt Lake City, Utah, USA; 2013. p. 4224.
56. Stanisz GJ, Kecojevic A, Bronskill MJ, Henkelman RM. Characterizing white matter with magnetization transfer and T2. Magn Reson Med. 1999;42(6):1128–36.
57. Ercan E, Varma G, Dimitrov IE, Xi Y, Pinho MC, Yu FF, et al. Combining inhomogeneous magnetization transfer and multipoint Dixon acquisition: Potential utility and evaluation. Magn Reson Med. 2021;85(4):2136–44.
58. Wood TC, Damestani NL, Lawrence AJ, Ljungberg E, Barker GJ, Solana AB, et al. Silent myelin-weighted magnetic resonance imaging. Vol. 5, Wellcome Open Res. 2020. p. 74.
59. Varma G, Munsch F, Burns B, Duhamel G, Girard OM, Guidon A, et al. Three-dimensional inhomogeneous magnetization transfer with rapid gradient-echo (3D ihMTRAGE) imaging. Magn Reson Med. 2020 Dec;84(6):2964–80.
60. Munsch F, Varma G, Taso M, Girard O, Guidon A, Duhamel G, et al. Characterization of the cortical myeloarchitecture with inhomogeneous magnetization transfer imaging (ihMT). NeuroImage. 2021 Jan 15;225:117442.
61. Taso M, Munsch F, Girard OM, Duhamel G, Alsop DC, Varma G. Improved volumetric inhomogeneous magnetization transfer (ihMT) using a CSF-suppressed FSE sequence (FLAIR-ihMT). In: Proceedings of the ISMRM. 2021. p. 717.
62. Curtis AT, Harris CT. Inhomogeneous Magnetization Transfer Steady State Imaging at 0.5T: Exploring SAR and B1+RMS envelope. In: Proceedings of the ISMRM. 2021. p. 0151.
63. Michal CA. Low-cost low-field NMR and MRI: Instrumentation and applications. J Magn Reson. 2020 Oct 1;319:106800.
64. Soustelle L, Lamy J, Troter AL, Hertanu A, Guye M, Ranjeva JP, et al. A Motion Correction Strategy for Multi-Contrast based 3D parametric imaging: Application to Inhomogeneous Magnetization Transfer (ihMT). bioRxiv. 2020 Sep 13;2020.09.11.292649.
65. Sled JG. Modelling and interpretation of magnetization transfer imaging in the brain. NeuroImage. 2018 Nov 15;182:128–35.
66. Varma G, Girard OM, Prevost V, Duhamel G, Alsop DC. Extracting a robust inhomogeneous magnetization transfer (ihMT) rate parameter, ihMT- R ex. In: Proceedings of the ISMRM. Toronto, Canada; 2015. p. 3357.
67. Helms G, Dathe H, Kallenberg K, Dechent P. High-resolution maps of magnetization transfer with inherent correction for RF inhomogeneity and T1 relaxation obtained from 3D FLASH MRI. Magn Reson Med. 2008 Dec;60(6):1396–407.
68. Zaiss M, Xu J, Goerke S, Khan IS, Singer RJ, Gore JC, et al. Inverse Z-spectrum analysis for spillover-, MT-, and T1 -corrected steady-state pulsed CEST-MRI--application to pH-weighted MRI of acute stroke.

NMR Biomed. 2014 Mar;27(3):240–52.
69. Zhang L, Chen T, Tian H, Xue H, Ren H, Li L, et al. Reproducibility of inhomogeneous magnetization transfer (ihMT): A test-retest, multi-site study. Magn Reson Imaging. 2019 Apr 1;57:243–9.
70. Zhang L, Wen B, Chen T, Tian H, Xue H, Ren H, et al. A comparison study of inhomogeneous magnetization transfer (ihMT) and magnetization transfer (MT) in multiple sclerosis based on whole brain acquisition at 3.0 T. Magn Reson Imaging. 2020 Jul 1;70:43–9.
71. Hou G, Lai W, Jiang W, Liu X, Qian L, Zhang Y, et al. Myelin deficits in patients with recurrent major depressive disorder: An inhomogeneous magnetization transfer study. Neurosci Lett. 2021 Apr 17;750:135768.
72. Chen G, Fu S, Chen P, Zhong S, Chen F, Qian L, et al. Reduced myelin density in unmedicated major depressive disorder: An inhomogeneous magnetization transfer MRI study. J Affect Disord. 2022 Mar 1;300:114–20.
73. Yarnykh VL. Optimal radiofrequency and gradient spoiling for improved accuracy of T1 and B1 measurements using fast steady-state techniques. Magn Reson Med. 2010 Jun;63(6):1610–26.
74. Mossahebi P, Yarnykh VL, Samsonov A. Analysis and Correction of Biases in Cross-Relaxation MRI due to Bi-Exponential Longitudinal Relaxation. Magn Reson Med. 2014 Feb;71(2):830–8.
75. Yarnykh VL. Actual flip-angle imaging in the pulsed steady state: A method for rapid three-dimensional mapping of the transmitted radiofrequency field. Magn Reson Med. 2007;57(1):192–200.
76. Sacolick LI, Wiesinger F, Hancu I, Vogel MW. B1 mapping by Bloch-Siegert shift. Magn Reson Med. 2010 May;63(5):1315–22.
77. Rowley CD, Campbell JSW, Wu Z, Leppert IR, Rudko DA, Pike GB, et al. A model-based framework for correcting inhomogeneity effects in magnetization transfer saturation and inhomogeneous magnetization transfer saturation maps. Magn Reson Med. 2021;86(4):2192–207.
78. Manning AP, MacKay AL, Michal CA. Understanding aqueous and non-aqueous proton T1 relaxation in brain. J Magn Reson San Diego Calif 1997. 2021 Feb;323:106909.
79. Wang Y, van Gelderen P, de Zwart JA, Duyn JH. B0-field dependence of MRI T1 relaxation in human brain. NeuroImage. 2020 Jun;213:116700.
80. West DJ, Cruz G, Teixeira RPAG, Schneider T, Tournier JD, Hajnal JV, et al. An MR fingerprinting approach for quantitative inhomogeneous magnetization transfer imaging. Magn Reson Med. 2022;87(1):220–35.
81. Morell P, Quarles RH. Characteristic Composition of Myelin. In: Siegel G, Agranoff B, Albers R, Fisher S, Uhler M, editors. Basic Neurochemistry: Molecular, Cellular and Medical Aspects 6th edition. Philadelphia: Lippincott-Raven; 1999.
82. Le Bras B, Chatzopoulou E, Heydon K, Martínez S, Ikenaka K, Prestoz L, et al. Oligodendrocyte development in the embryonic brain: the contribution of the plp lineage. Int J Dev Biol. 2005;49(2–3):209–20.
83. Spassky N, Olivier C, Cobos I, LeBras B, Goujet-Zalc C, Martínez S, et al. The early steps of oligodendrogenesis: insights from the study of the plp lineage in the brain of chicks and rodents. Dev Neurosci. 2001;23(4–5):318–26.
84. West DJ, Teixeira RPAG, Wood TC, Hajnal JV, Tournier JD, Malik SJ. Inherent and unpredictable bias in multi-component DESPOT myelin water fraction estimation. NeuroImage. 2019 Jul 15;195:78–88.
85. Van Obberghen E, Mchinda S, Troter A le, Prevost VH, Viout P, Guye M, et al. Evaluation of the Sensitivity of Inhomogeneous Magnetization Transfer (ihMT) MRI for Multiple Sclerosis. Am J Neuroradiol. 2018 Apr 1;39(4):634–41.
86. Rasoanandrianina H, Demortière S, Trabelsi A, Ranjeva JP, Girard O, Duhamel G, et al. Sensitivity of the Inhomogeneous Magnetization Transfer Imaging Technique to Spinal Cord Damage in Multiple Sclerosis. Am J Neuroradiol. 2020 May 1;41(5):929–37.
87. Taso M, Girard OM, Duhamel G, Le Troter A, Feiweier T, Guye M, et al. Tract-specific and age-related variations of the spinal cord microstructure: a multi-parametric MRI study using diffusion tensor imaging (DTI) and inhomogeneous magnetization transfer (ihMT). NMR Biomed. 2016 Jun;29(6):817–32.
88. Rasoanandrianina H, Grapperon AM, Taso M, Girard OM, Duhamel G, Guye M, et al. Region-specific impairment of the cervical spinal cord (SC) in amyotrophic lateral sclerosis: A preliminary study using SC templates and quantitative MRI (diffusion tensor imaging/inhomogeneous magnetization transfer). NMR Biomed. 2017 Dec;30(12).